Publication Year	2015
Acceptance in OA@INAF	2021-01-14T14:28:01Z
Title	Testing Gravity with Quasi-periodic Oscillations from Accreting Black Holes: The Case of Einstein-Dilaton-Gauss-Bonnet Theory
Authors	MASELLI, ANDREA; Gualtieri, Leonardo; Pani, Paolo; STELLA, Luigi; Ferrari, Valeria
DOI	10.1088/0004-637X/801/2/115
Handle	http://hdl.handle.net/20.500.12386/29771
Journal	THE ASTROPHYSICAL JOURNAL
Number	801

The Astrophysical Journal, 801:115 (9pp), 2015 March 10 doi:10.1088/0004-637X/801/2/115
© 2015. The American Astronomical Society. All rights reserved.

TESTING GRAVITY WITH QUASI-PERIODIC OSCILLATIONS FROM ACCRETING BLACK HOLES: THE CASE OF THE EINSTEIN–DILATON–GAUSS–BONNET THEORY

Andrea Maselli[1], Leonardo Gualtieri[1], Paolo Pani[2,1], Luigi Stella[3], and Valeria Ferrari[1]
[1] Dipartimento di Fisica, Universitàdi Roma "La Sapienza" & Sezione INFN Roma1, P.A. Moro 5, I-00185, Roma, Italy
[2] CENTRA, Departamento de Física, Instituto Superior Técnico, Universidade de Lisboa, Avenida Rovisco Pais 1, 1049 Lisboa, Portugal
[3] INAF-Osservatorio Astronomico di Roma, via di Frascati 33, I-00040, Monteporzio Catone, Roma, Italy
Received 2014 December 10; accepted 2015 January 11; published 2015 March 12

ABSTRACT

Quasi-periodic oscillations (QPOs) observed in the X-ray flux emitted by accreting black holes are associated with phenomena occurring near the horizon. Future very large area X-ray instruments will be able to measure QPO frequencies with very high precision, thus probing this strong-field region. Using the relativistic precession model, we show the way in which QPO frequencies could be used to test general relativity (GR) against those alternative theories of gravity which predict deviations from the classical theory in the strong-field and high-curvature regimes. We consider one of the best-motivated high-curvature corrections to GR, namely, the Einstein–Dilaton–Gauss–Bonnet theory, and show that a detection of QPOs with the expected sensitivity of the proposed ESA M-class mission *LOFT* would set the most stringent constraints on the parameter space of this theory.

Key words: accretion, accretion disks – black hole physics – gravitation – X-rays: binaries

1. INTRODUCTION

Since its formulation a century ago, general relativity (GR) has successfully passed a number of observational and experimental tests (Will 2014). However, since these tests mostly probed the weak-field regime of gravity, a number of strong-field/high-curvature GR predictions still remain to be verified (Psaltis 2008; Yunes & Siemens 2013).

Astrophysical systems involving collapsed objects, i.e., black holes (BHs) and neutron stars (NSs), provide us with ways to study the properties of the strong gravitational fields in their close surroundings. Most of the radiation emitted by matter accreting onto BHs and NSs originates very deep in the gravitational fields of these objects, at distances down to a few gravitational radii $r_g = GM/c^2$. The motion of this matter holds the potential to study the properties of gravity in the strong-field regime and to verify some of the yet untested and key predictions of GR. X-ray observations of matter accretion onto stellar mass BHs and NSs in binary systems and onto supermassive BHs in active galactic nuclei (AGNs) have singled out a few powerful diagnostics over the last two decades. Spectral diagnostics include the soft X-ray continuum emission of accretion disks, whose highest temperature has been used to measure the innermost disk radius, likely extending to the innermost stable circular orbit (ISCO), and thus to infer the spin of stellar mass BHs (for a review see McClintock et al. 2011). The extremely broad and redshifted iron Kα line around ~6 keV, observed in X-ray binaries as well as AGNs, has been extensively exploited for the same purpose; it also carries key information about the dynamics, emissivity, and geometrical properties of the inner disk regions (for a recent review see Fabian et al. 2013). Tests of GR based on observations of the soft X-ray continuum emission and of the iron Kα line in BH accretion disks have been discussed, e.g., in Bambi & Barausse (2011), Johannsen & Psaltis (2013), and Bambi (2013a).

Very fast flux variability produced by matter orbiting close to BHs and NSs has long been considered a potential probe of geodetic motion in the strong-field regime (e.g., Syunyaev 1972). Moreover, for stellar-mass BHs it also probes the high-curvature regime of the theory.

This diagnostic only began to come to fruition in the late 90s, when fast quasi-periodic oscillations (QPOs) at X-ray energies and with frequencies close to those expected from bound orbits at characteristic radii of $\lesssim 10\ r_g$ were discovered. Different QPO modes excited at the same time were studied in a number of NS X-ray binaries, whose variable frequency extended to >1 kHz in the highest mode. A similar QPO phenomenology was observed in several BH X-ray binaries where frequencies up to ~450 Hz were detected (for a review see van der Klis 2006). In a few cases, QPOs were also detected in the X-ray flux of supermassive AGNs (e.g., Gierliński et al. 2008). Several models have been proposed to interpret the QPO phenomenon, virtually all of them involving the fundamental frequencies of motion of matter in the strong-field regime; these are drastically different from their Newtonian equivalent, such that no weak field expansion of GR can approximate them (for a recent review see Belloni & Stella 2014 and references therein).

The QPO signals can provide a powerful diagnostic of strong gravitational fields and for regions with high curvature; BHs are especially promising in this respect, by virtue of their simplicity. First, the so-called *no-hair theorems* (see, e.g., Hawking & Ellis 1973 and references therein) demonstrated that the spacetime of a stationary BH in GR depends only on its mass and angular momentum. Second, unlike NSs, BHs do not possess stable magnetic fields, or a "hard" surface or boundary layer that can alter considerably the dynamics of matter inflow at the smallest radii. Simultaneous QPO modes in BHs have so far been detected only in a few cases; moreover, the accuracy of the corresponding frequency measurements is limited to $>1-2\%$. Despite these limitations, the application of the Relativistic Precession Model (RPM, see Section 2.1) to the QPOs from the BH X-ray binary GRO J1655-40 (Motta et al. 2014), the only BH binary system in which three simultaneous QPOs were observed, yielded precise measurements of the BH mass and spin, the former being in full agreement with the mass derived from optical observations.

With the development of very high throughput X-ray instrumentation, it is expected that simultaneous QPO signals will be detected in a variety of BHs and their frequency will be measured to high precision and accuracy, such that quantitative tests of GR predictions in the strong-field/high-curvature regime will become feasible. X-ray astronomy satellites that can achieve these goals have been actively studied in recent years. In particular, the proposed ESA X-ray satellite *LOFT*, with its extremely high effective area (up to $\sim 10\,\mathrm{m}^2$) and good CCD-type spectral resolution (~ 180 eV) in the classical X-ray range (2–50 keV), offers the best prospects for exploiting the QPO diagnostic (Feroci et al. 2012).

As with other astrophysical systems (e.g., the pulse timing of relativistic binary pulsars (Kramer 2014) and extreme mass-ratio inspirals (Amaro-Seoane et al. 2014)), QPOs provide in principle two different methods to test GR. In the first method, GR predictions are directly compared to measurements and tested for consistency. In the second method, alternative theories are introduced, and their parameters are constrained to demonstrate whether GR is confirmed as the best theory of gravity.

Some degree of "redundancy" is required in order to apply the second method, in that the measurements must be sufficient to constrain (or infer) more parameters than those required by GR alone. In this context, alternative gravity theories have been introduced by adopting two different approaches (Psaltis 2009). In a bottom-up approach, one parametrizes the BH spacetime in a phenomenological way and, once a deviation from GR is found (or constrained) in terms of these parameters, one tries to interpret such a deviation (or constraint) in terms of an alternative theory. However, the parametrizations that have been proposed in the literature up to now either do not reproduce BH solutions of known theories alternative to GR (Collins & Hughes 2004; Glampedakis & Babak 2006; Johannsen & Psaltis 2010) or are very involved, and therefore are to some extent impractical (Vigeland et al. 2011). In a top-down approach, instead, one considers modifications of GR, possibly inspired by fundamental physics considerations, and then works out the predictions of such modifications to be tested against observation. We adopt here a top-down approach to calculate the modified fundamental frequencies of motion that underlay QPO models. We mention that bottom-up approaches have been employed to test GR using QPO signals from accreting BHs in Johannsen & Psaltis (2011) and Bambi (2012, 2013b).

Among the gravity theories that have been proposed as alternatives to GR (see, e.g., the reviews of Psaltis 2008; Yunes & Siemens 2013; Will 2014), we the select Einstein–Dilaton–Gauss–Bonnet (EDGB) theory (Kanti et al. 1996), in which the Gauss–Bonnet invariant

$$\mathcal{R}^2_{\rm GB} = R_{\alpha\beta\delta\gamma}R^{\alpha\beta\delta\gamma} - 4R_{\alpha\beta}R^{\alpha\beta} + R^2 \qquad (1)$$

is included in the action, coupled with a scalar field. The reasons for this choice are as follow.

1. The most natural way to modify the strong-field /high-curvature regime of gravity is to include in the action a quadratic term in the curvature tensor.
2. If the equations of motion have third- (or higher) order derivatives, then the theory is subject to Ostrogradsky's instability (Woodard 2007). The Gauss–Bonnet invariant is the only quadratic term in the curvature which leads to second-order field equations, thus avoiding this instability. Theories with quadratic curvature invariants different from (1) should be treated as effective theories, in which higher-order terms are assumed to be present in the action and neglected in some regime.
3. Since $\mathcal{R}^2_{\rm GB}$ is a total derivative, it would not contribute to the field equations unless it is coupled to a scalar field, as in the EDGB theory.
4. The Gauss–Bonnet term can be seen as the first term in an expansion including all possible curvature invariants and their powers, as suggested by low-energy effective string theories (see, e.g., Moura & Schiappa 2007 and references therein).
5. Scalar–tensor theories which do not include quadratic (or higher) curvature invariants (see e.g., Fujii et al. 2003 and references therein) do not introduce strong-field /high curvature corrections to GR.[4] Moreover, stationary BHs in these theories satisfy the no-hair theorems of GR (Sotiriou & Faraoni 2012). It is then impossible to test GR against these theories using BHs close to stationarity. Similar results apply to $f(R)$ theories. In the EDGB theory, instead, BH solutions are different from those of GR (Mignemi & Stewart 1993; Kanti et al. 1996; Pani & Cardoso 2009; Yunes & Stein 2011; Sotiriou & Zhou 2014). Testing these differences is the goal of this work.

In this paper, we calculate the azimuthal and epicyclic frequencies of a slowly rotating BH in EDGB gravity and find that these differ from their GR equivalent by up to $\sim 4\%$. A similar computation has been carried out for dynamical Chern-Simons gravity (a different theory with quadratic curvature terms, see Alexander & Yunes 2009 for a review) in Vincent (2013), finding that deviations from GR predicted by that theory are much smaller. Using the RPM, we show that the differences between the QPO frequencies predicted by GR and EDGB gravity, while undetectable with currently available BH QPO measurements, can be large enough to be measured with the next generation of large area X-ray instruments. The paper is organized as follows. In Section 2, we summarize the RPM and the procedure for computing the azimuthal and epicyclic frequencies in BH spacetime. In Section 3, we briefly discuss EDGB gravity, the solutions of this theory describing slowly rotating BHs, the geodesics in this spacetime, and the approach to compute the epicyclic frequencies. In Section 4, we compute the QPO frequencies in EDGB gravity and show how they can be used to test GR against EDGB theory. Finally, in Section 5, we draw the conclusions.

2. QUASI-PERIODIC OSCILLATIONS IN THE X-RAY FLUX OF ACCRETING BHS

Most QPO models were originally proposed in the context of accreting NSs, with the faster of the twin kHz QPO modes often being interpreted as arising from the azimuthal motion of matter in the inner disk region (for a review see van der Klis 2000). When BH QPOs were discovered, it was realized that despite their relatively low amplitudes and simpler phenomenology, they provided a "cleaner" environment to study the properties of strong gravitational fields and high-curvature regions, through the motion of matter that generates the QPOs.

Building on the similarity between the QPO modes that are observed in NSs and BHs, especially the presence of a QPO

[4] Except in the case of neutron stars-for specific solutions, for instance, such as those discussed in Damour & Esposito-Farèse (1993).

pair at higher frequencies, a few models were applied to both types of systems. Especially successful among these are the RPM, which we base our analysis on here, and the epicyclic resonance model (Kluzniak & Abramowicz 2001; Abramowicz & Kluźniak 2001) which will be discussed in future work.

2.1. The Relativistic Precession Model

The RPM was formulated in order to interpret the twin QPOs around ∼1 kHz as well as a low-frequency QPO mode (the so-called Horizontal Branch Oscillations, HBOs) of NSs in low-mass X-ray binaries (Stella & Vietri 1998, 1999). The higher- and lower-frequency kHz QPOs are identified with the azimuthal frequency ν_φ, and the periastron precession frequency, $\nu_{\rm per} = \nu_\varphi - \nu_r$, of matter orbiting in quasi-circular orbits at a given radius r of the innermost disk region, with ν_r being the radial epicyclic frequency. The low-frequency QPO mode is instead related to the nodal precession frequency, $\nu_{\rm nod} = \nu_\varphi - \nu_\theta$, where ν_θ is the vertical epicyclic frequency. $\nu_{\rm nod}$ is emitted at the same radius where the signals at ν_φ and $\nu_{\rm per}$ are produced. Correlated QPO frequency variations that are observed from individual NSs at different times are well reproduced in the RPM as a result of variations in the radius at which the QPOs are emitted.

The RPM was first applied to BH systems by Stella et al. (1999). A complete application to BHs involving three QPO modes became possible only recently, following the realization that in GRO J1655-40 the BH equivalent of the HBOs, the so-called type C low-frequency QPOs (Casella et al. 2005), in one instance were detected simultaneously with two high-frequency QPOs (see Motta et al. 2014 and references therein). The centroid frequency of these QPOs was measured by the PCA on board the *Rossi X-Ray Timing Explorer* (*RXTE*) with 1σ uncertainties in the 1–2% range. Their values are

$$\nu_\varphi = 441^{+2}_{-2}\ Hz,\ \ \nu_{\rm per} = 298^{+4}_{-4}\ Hz,\ \ \nu_{\rm nod} = 17.3^{+0.1}_{-0.1}\ Hz, \quad (2)$$

where the ν symbols refer to the RPM interpretation. By fitting the three simultaneous QPOs (hereafter the QPO triplet) with the RPM frequencies from the Kerr metric, precise values of $M = (5.31 \pm 0.07)\, M_\odot$, $a^\star = J/M^2 = 0.290 \pm 0.003$, and the radius[5] from which the QPO triplet originated were obtained through the sole use of X-ray timing.

The former value is fully consistent with the BH mass as inferred from optical/NIR spectro-photometric observations, $(5.4 \pm 0.3)\, M_\odot$ (Beer & Podsiadlowski 2002). The QPO radius was found to be $(5.68 \pm 0.04) r_g$, i.e., only ∼13% larger than R_{ISCO}, very deep in the gravitational field of the BH.[6]

The detection of a single QPO triplet yields only the above-mentioned three quantities with no redundancy. The relative width of the three power spectrum QPO peaks in GRO J1655-40 was found to be consistent with being due to jitter variations of the radius where QPOs are generated, suggesting that future, high-throughput X-ray observations can reveal frequency variations of the QPO triplet as a function of time in accreting BH systems. If more triplets are detected, then additional information concerning the properties of the strong-field/high-curvature gravity very close to BHs can be derived: for instance, it would be possible to study the radial dependence of the fundamental frequencies. Since the signal-to-noise ratio of incoherent power spectrum signals (such as QPOs) scales linearly with the rates in photon counting instruments, larger area X-ray detectors of the future will provide a correspondingly higher precision in QPO measurement. Our calculations here are based on the *LOFT*-LAD instrument which, due to its effective area, will provide a factor of ∼15 improved precision relative to the *RXTE*-PCA values quoted above (see Equation (2)).

2.2. The Epicyclic Frequencies of a Rotating Black Hole

Here, we derive the expressions for the epicyclic frequencies (see also Wald 2010; Merloni et al. 1999; Abramowicz & Kluzniak 2003; Vincent 2013). In this derivation, we only require that the spacetime is stationary, axisymmetric, circular (i.e., invariant to the simultaneous inversion of time and of the azimuthal angle ϕ), and symmetric across the equatorial plane. Circularity and equatorial symmetry are satisfied by (stationary, axisymmetric) BH solutions in GR and by most BH solutions in alternative theories of gravity; in particular, they are satisfied by (stationary, axisymmetric) BH solutions in EDGB gravity.

The metric of a stationary, axially symmetric spacetime which satisfies the circularity condition can be expressed in the form (see e.g., Chandrasekhar 1984)

$$ds^2 = g_{tt}dt^2 + g_{rr}dr^2 + g_{\theta\theta}d\theta^2 + 2g_{t\varphi}dtd\varphi + g_{\varphi\varphi}d\varphi^2, \quad (3)$$

where $g_{\mu\nu} = g_{\mu\nu}(r, \theta)$. Let $u^\mu = \dot{x}^\mu = dx^\mu/d\tau$ be the four-velocity of a massive particle (τ being the proper time). Stationarity and axisymmetry imply that there are two constants of geodesic motion, $E = -u_t$ and $L = u_\varphi$, which we refer to as the energy and the angular momentum per unit mass of the moving particle. We also define the proper angular momentum $l = L/E$, and the potential

$$\mathcal{U}(r, \theta) = g^{tt} - 2lg^{t\varphi} + l^2\, g^{\varphi\varphi}. \quad (4)$$

Since $g^{\mu\nu}u_\mu u_\nu = -1$,

$$g_{rr}\dot{r}^2 + g_{\theta\theta}\dot{\theta}^2 + E^2\mathcal{U}(r, \theta) = -1. \quad (5)$$

If we consider equatorial motion, then Equation (5) gives $\dot{r}^2 = V(r)$, where $V(r) = -g_{rr}^{-1}E^2\left[E^2\mathcal{U}(r, \pi/2) + 1\right]$ is an effective potential.

For a circular, equatorial orbit at $r = \bar{r}$, $\dot{r} = 0$ and, from Equation (5), we get $\mathcal{U}_{,r}(\bar{r}, \pi/2) = \mathcal{U}_{,\theta}(\bar{r}, \pi/2) = 0$. E and L can be determined by imposing $V(\bar{r}) = V'(\bar{r}) = 0$, where the prime indicates differentiation with respect to r and the further condition $V'' = 0$ yields the ISCO radius. The four-velocity on a circular, equatorial orbit has the form $u^\mu = u^0(1, 0, 0, \Omega)$, where the angular velocity $\Omega = 2\pi\nu_\varphi$ can be found by solving the algebraic equation

$$g_{tt,r} + 2\Omega g_{t\varphi,r} + \Omega^2 g_{\varphi\varphi,r} = 0. \quad (6)$$

Let us now consider a small perturbation of a circular, equatorial orbit, i.e.,

$$r(t) = \bar{r} + \delta r(t) \qquad \theta(t) = \frac{\pi}{2} + \delta\theta(t) \quad (7)$$

with $\delta r \sim e^{2\pi i\nu_r t}$, $\delta\theta \sim e^{2\pi i\nu_\theta t}$, and $\delta r \ll \bar{r}$, $\delta\theta \ll \pi/2$. ν_φ, ν_r, and ν_θ are the azimuthal and the epicyclic frequencies.

[5] M and J are the Arnowitt–Deser–Misner BH mass and angular momentum, respectively.

[6] For the values above, the BH event horizon is at 1.96 M.

Equation (5) yields

$$-g_{rr}\left(u^0 2\pi\nu_r\delta r\right)^2 - g_{\theta\theta}\left(u^0 2\pi\nu_\theta\delta\theta\right)^2 + E^2\left[\mathcal{U}\left(\bar{r},\frac{\pi}{2}\right) + \frac{1}{2}\frac{\partial^2\mathcal{U}}{\partial r^2}\left(\bar{r},\frac{\pi}{2}\right)\delta r^2 + \frac{1}{2}\frac{\partial^2\mathcal{U}}{\partial\theta^2}\left(\bar{r},\frac{\pi}{2}\right)\delta\theta^2\right] = 0. \quad (8)$$

Since $E = -(g_{tt} + \Omega g_{t\varphi})u^0$, Equation (8) implies

$$\nu_r^2 = \frac{\left(g_{tt} + \Omega g_{t\varphi}\right)^2}{2(2\pi)^2 g_{rr}}\frac{\partial^2\mathcal{U}}{\partial r^2}\left(\bar{r},\frac{\pi}{2}\right),$$

$$\nu_\theta^2 = \frac{\left(g_{tt} + \Omega g_{t\varphi}\right)^2}{2(2\pi)^2 g_{\theta\theta}}\frac{\partial^2\mathcal{U}}{\partial\theta^2}\left(\bar{r},\frac{\pi}{2}\right). \quad (9)$$

3. SPINNING BHs IN EINSTEIN–DILATON–GAUSS–BONNET GRAVITY

In this Section, we briefly describe the EDGB theory and its slowly rotating BH solution.

3.1. EDGB Gravity

EDGB theory is defined by the following action (Kanti et al. 1996):[7]

$$S = \frac{1}{2}\int d^4x\sqrt{-g}\left[R - \frac{1}{2}\partial_\mu\phi\partial^\mu\phi + \frac{\alpha e^\phi}{4}\mathcal{R}^2_{\rm GB}\right], \quad (10)$$

where the Gauss–Bonnet invariant $\mathcal{R}^2_{\rm GB}$ is defined as in Equation (1) and $\alpha > 0$ is a coupling constant (in the framework of string theory, α corresponds to the Regge slope; the gauge coupling constant has been fixed to 1). We use units in which $G = c = 1$; with this choice, the scalar field ϕ is dimensionless and α has the dimension of a squared length.

The field equations of the EDGB theory are found varying the action (10) with respect to $g_{\mu\nu}$ and ϕ:

$$G_{\mu\nu} = \frac{1}{2}\partial_\mu\phi\partial_\nu\phi - \frac{1}{4}g_{\mu\nu}\partial_\alpha\phi\partial^\alpha\phi - \alpha\mathcal{K}_{\mu\nu}, \quad (11)$$

$$\frac{1}{\sqrt{g}}\partial_\mu\left(\sqrt{g}\,\partial^\mu\phi\right) = -\frac{\alpha}{4}e^\phi\mathcal{R}^2_{\rm GB}, \quad (12)$$

where $G_{\mu\nu} = R_{\mu\nu} - \frac{1}{2}g_{\mu\nu}R$ is the Einstein tensor,

$$\mathcal{K}_{\mu\nu} = \frac{g_{\mu\rho}g_{\nu\lambda} + g_{\mu\lambda}g_{\nu\rho}}{8}\epsilon^{k\lambda\alpha\beta}\nabla_\gamma\left(\epsilon^{\rho\gamma\mu\nu}R_{\mu\nu\alpha\beta}\partial_k e^\phi\right), \quad (13)$$

and $\epsilon^{0123} = -(-g)^{-1/2}$.

The solution of Equations (11) and (12) describing a spherically symmetric BH was found by solving the field equations numerically in Kanti et al. (1996). An analytical solution has been derived to second order in α/M^2 in Mignemi & Stewart (1993) and Yunes & Stein (2011).

3.2. Slowly Rotating Black Holes

The solution of the EDGB Equations (11) and (12) which describes a slowly rotating BH was derived in Pani & Cardoso (2009). It was obtained as a perturbation of the spherically symmetric, non-rotating BH solution derived in Kanti et al. (1996) to first order in the BH spin $a^\star = J/M^2$. This solution (as in the non-rotating case) only exists if

$$e^{\phi_{\rm h}} \leqslant \frac{r_{\rm h}^2}{\alpha\sqrt{6}}, \quad (14)$$

where $r_{\rm h}$ and ϕ_h are the radial coordinate and the scalar field evaluated at the horizon. We refer the reader to the Appendix of Kanti et al. (1996) for an explicit derivation of the equations of motion of the spherically symmetric solution. From the asymptotic behavior of the metric, we can extract M and the dilatonic charge D. Since the field equations are invariant under the rescaling $\phi \to \phi + \phi_0$, $r \to re^{\phi_0/2}$ (or equivalently $M \to Me^{\phi_0/2}$, $D \to De^{\phi_0/2}$), for each value of M there is only one solution to the non-rotating BH; the dilatonic charge can be determined in terms of the BH mass.

As noted in Pani & Cardoso (2009), by imposing asymptotic flatness (i.e., $\lim_{r\to\infty}\phi = 0$), condition (14) can be written as

$$0 < \frac{\alpha}{M^2} \lesssim 0.691. \quad (15)$$

The best observational bound on the coupling parameter was derived by Yagi (2012) using the orbital decay rate of low-mass X-ray binaries and reads[8] $\alpha \lesssim 47\,M_\odot^2$, which is weaker than the theoretical bound (15) for BHs with $M \lesssim 8.2\,M_\odot$. Constraints of the same order of magnitude were obtained in Pani et al. (2011a) by studying slowly rotating NSs in the EDGB theory, but they are limited by the uncertainties on the NS equation of state. Thus, the range defined by the theoretical bound (15) is unconstrained to date (at least, for BHs with $M \lesssim 8.2\,M_\odot$).

The spacetime metric of a slowly rotating BH at first order in the angular momentum can be written as

$$ds^2 = -f(r)dt^2 + \frac{dr^2}{g(r)} + r^2\left(d\theta^2 + \sin^2\theta d\varphi^2\right) - 2r^2\sin^2\theta\omega(r)dtd\varphi. \quad (16)$$

Equations (11) and (12) yield a set of differential equations which allow us to compute the metric functions $f(r)$, $g(r)$, $\omega(r)$, and the scalar profile $\phi(r)$. The equations for $f(r)$, $g(r)$, and $\phi(r)$ coincide with those of a non-rotating BH, which are discussed in Kanti et al. (1996); the equation for $\omega(r)$ has the form

$$\omega''(r) + \frac{G_1(r)}{G_2(r)}\omega'(r) = 0, \quad (17)$$

where

$$G_1(r) = -\frac{r^2}{g}\left[\frac{f'}{f} - \frac{g'}{g} - \frac{8}{r}\right] - \phi'\left[\frac{6}{r} - \frac{f'}{f} + \frac{3\,g'}{g} + 2\phi'\right] + 2e^\phi r\phi'' \quad (18)$$

$$G_2(r) = 2r^2\,g^{-1} - 2\,re^\phi\phi'. \quad (19)$$

The solution of Equation (17) can be written as

[7] Note that we use the same signature as in Kanti et al. (1996), but the opposite sign convention for the definition of the Riemann tensor.

[8] This corresponds to the bound $\sqrt{\alpha} < 1.9$ km derived in Yagi (2012) from observations of the low-mass X-ray binary A0620-00. Note also that this bound was obtained by truncating the EDGB theory to first order in the coupling, and does not necessarily hold in the full theory that we are studying here. In order to convert our notation and conventions to those of Yagi (2012), we should replace $\phi \to \sqrt{16\pi}\,\phi$ and $\alpha \to 16\sqrt{\pi}\,\alpha$.

Table 1
Relative Difference Between the Values of the Azimuthal/Epicyclic Frequencies Derived in GR and in EDGB Gravity, Computed at the Emission Radius $r = 1.1\, r_{\rm ISCO}$, for $M = 5.3\, M_\odot$, $a^\star = (0.02, 0.05, 0.1)$, and Different Choices of α/M^2

	$a^\star = 0.02$					$a^\star = 0.05$					$a^\star = 0.1$				
α/M^2	ϵ_φ %	ϵ_r %	ϵ_θ %	$\epsilon_{\rm nod}$ %	$\epsilon_{\rm per}$ %	ϵ_φ %	ϵ_r %	ϵ_θ %	$\epsilon_{\rm nod}$ %	$\epsilon_{\rm per}$ %	ϵ_φ %	ϵ_r %	ϵ_θ %	$\epsilon_{\rm nod}$ %	$\epsilon_{\rm per}$ %
0.691	2.66	1.07	2.65	7.4	3.34	2.85	1.16	2.82	9.5	3.58	3.26	1.37	3.16	13.0	4.06
0.576	1.30	0.55	1.30	4.6	1.63	1.43	0.62	1.40	6.7	1.78	1.73	0.80	1.64	10.2	2.12
0.418	0.58	0.26	0.58	3.2	0.72	0.67	0.32	0.65	5.2	0.82	0.91	0.50	0.83	8.6	1.09
0.237	0.18	0.07	0.17	2.3	0.22	0.26	0.11	0.23	4.3	0.32	0.47	0.23	0.34	7.7	0.57
0.104	0.05	0.03	0.04	1.8	0.05	0.11	0.08	0.09	3.9	0.12	0.31	0.23	0.23	7.2	0.34
0.0529	0.03	0.02	0.02	2.0	0.03	0.10	0.07	0.08	4.0	0.11	0.30	0.21	0.23	7.4	0.34
0.00298	0.02	0.00	0.01	1.8	0.02	0.08	0.04	0.06	3.8	0.10	0.27	0.16	0.20	7.2	0.32

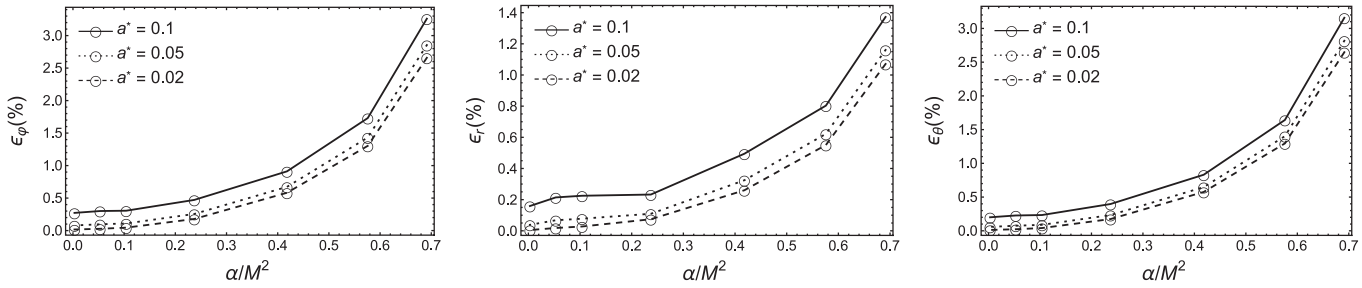

Figure 1. Relative difference between the azimuthal/epicyclic frequencies (ν_φ, ν_r, ν_θ) computed in GR and in the EDGB theory plotted as a function of the coupling constant α/M^2 for different values of the BH spin parameter $a^\star = (0.02, 0.05, 0.1)$. All quantities are computed at $r = 1.1\, r_{\rm ISCO}$.

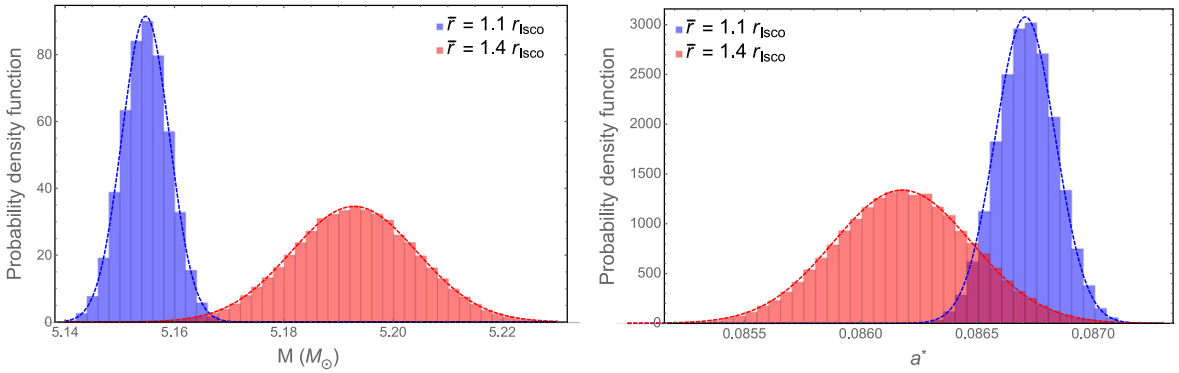

Figure 2. Distribution of the BH mass M (left panel) and spin $a^\star$ (right panel) as obtained from the measurement of the epyciclic frequencies (ν_φ, $\nu_{\rm per}$, $\nu_{\rm nod}$) at two different radii r. The generated frequencies follow Gaussian distributions with relative widths 15 times lower than those measured with the *RXTE*/PCA from GRO J1655-40, as expected for the *LOFT*-LAD instrument. A BH mass $\bar{M} = 5.3\, M_\odot$ and spin parameter $\bar{a}^\star = 0.1$ are adopted here in EDGB gravity with the maximal coupling constant ($\alpha/\bar{M}^2 = 0.691$).

$$\omega(r) = C_1 + C_2 \int^r ds\; e^{-\int^s G_2/G_3 dl}, \tag{20}$$

where C_1 and C_2 are integration constants. Since $f(r)$, $g(r)$, and $\phi(r)$ are known to be the result of numerical integrations, Equation (17) has to be solved numerically as well.[9]

Imposing the constraint that the spacetime is asymptotically flat, we obtain the asymptotic behavior

$$\omega(r) \sim \frac{2J}{r^3}. \tag{21}$$

For any given value of J, Equation (21) and its first derivative allow us to fix the integration constants C_1 and C_2.

[9] In the small coupling limit, where $f(r)$, $g(r)$, and $\phi(r)$ are known analytically, Equation (17) has been obtained in closed form in Pani et al. (2011b). The analytic, small coupling solution has been extended to second order in the spin by Ayzenberg & Yunes (2014).

The solution of (16) has the form (3), with $g_{tt} = -f(r)$, $g_{rr} = 1/g(r)$, $g_{\theta\theta} = r^2$, $g_{\varphi\varphi} = r^2 \sin^2\theta$, and $g_{t\varphi} = -r^2 \sin^2\theta\omega(r)$, and it is symmetric across the equatorial plane; therefore, the expressions of the azimuthal and epicyclic frequencies (ν_φ, ν_r, and ν_θ) presented in Section 2.1 also hold for solution (16). Finally, as discussed in Section 2.1, we define the periastron and nodal precession frequencies:

$$\nu_{\rm nod} = \nu_\varphi - \nu_\theta, \quad \nu_{\rm per} = \nu_\varphi - \nu_r. \tag{22}$$

4. RESULTS

4.1. Epicyclic Frequencies in EDGB Gravity

We have computed the frequencies ν_φ, ν_r, ν_θ, $\nu_{\rm per}$, and $\nu_{\rm nod}$ of a slowly rotating BH in EDGB gravity as functions of the BH mass and angular momentum, and of the coupling constant α/M^2. The solution discussed in Section 3.2 describes rotating

BHs to first order in the spin $a^\star$. Therefore, our results are affected by a relative error of the order of $\sim a^{\star 2}$.

In Table 1 and in Figure 1, we show the relative difference between the frequencies computed according to GR and to the EDGB theory,

$$\epsilon_i = \frac{\nu_i^{\rm EDGB} - \nu_i^{\rm GR}}{\nu_i^{\rm GR}} \qquad i = \varphi,\, r,\, \theta,\, {\rm nod},\, {\rm per}, \tag{23}$$

for different values of α/M^2 and $a^\star$. We assume a fiducial value of the BH mass $M = 5.3\, M_\odot$, corresponding to the estimated mass of GRO J1655-40 (Motta et al. 2014), and an emission radius $r = 1.1\, r_{\rm ISCO}$. The frequencies $\nu_i^{\rm GR}$ are those obtained using the Kerr metric, and are given by

$$\nu_\varphi^{\rm GR} = \frac{1}{2\pi}\frac{M^{1/2}}{r^{3/2} + a^\star M^{3/2}}, \tag{24}$$

$$\nu_r^{\rm GR} = \nu_\varphi^{\rm GR}\left(1 - \frac{6M}{r} + 8a^\star\frac{M^{3/2}}{r^{3/2}} - 3a^{\star 2}\frac{M^2}{r^2}\right)^{1/2}, \tag{25}$$

$$\nu_\theta^{\rm GR} = \nu_\varphi^{\rm GR}\left(1 - 4a^\star\frac{M^{3/2}}{r^{3/2}} + 3a^{\star 2}\frac{M^2}{r^2}\right)^{1/2}. \tag{26}$$

In the following, consistent with the slow-rotation approximation, we will consider Equations (24)–(26) expanded to first order in $a^\star$.

As shown in Table 1 and Figure 1, the deviations increase with α/M^2 and with the BH spin $a^\star$. They reach values as high as $\sim 1 - 4\%$; only $\epsilon_{\rm nod}$ can be as high as $\sim 13\%$. We also find that each $\nu_i^{\rm GR}$ is always smaller than the corresponding $\nu_i^{\rm EDGB}$, and thus all ϵ_i are greater than zero. We note that since we neglect $O(a^{\star\,2})$ terms, the $\alpha/M^2 \to 0$ limit of our results differs from GR by terms of the same order, with the exception of $\nu_{\rm nod}$, which is proportional to $a^\star$ and therefore has a relative error of $\epsilon_{\rm nod} \propto a^\star$. This should be considered as an order-of-magnitude estimate of the errors, since we do not know the $O((a^\star)^2)$ terms in the frequencies $\nu_i^{\rm EDGB}$ when $\alpha \neq 0$.

4.2. Testing Gravity with LOFT

According to the RPM, the three simultaneous QPO frequencies $(\nu_\varphi, \nu_{\rm per}, \nu_{\rm nod})$ are all generated at the same radial coordinate in the accretion flow. For each such triplet, the GR Equations (24)–(26) provide a system of three equations for the three unknown parameters $(M, a^\star, r)$ which can be solved analytically. In EDGB modified gravity, however, the coupling parameter α/M^2 which measures deviations from GR enters as an extra unknown parameter. In general, at least one more QPO triplet would be required in the RPM in order also to derive the α/M^2 parameter.[10]

As we noted in Section 2.1, it is expected that the *LOFT* very high effective area will allow for the detection of multiple QPO triplets corresponding to different radii in individual stellar mass BHs.

[10] In principle, if an independent, very precise measurement of the BH mass M were available, then a single triplet would suffice. The precision would have to be 1% or better, see Figure 2 (left panel). This compares unfavorably with the precision afforded by present optical/NIR mass measurements, see, e.g., Özel et al. (2010) and references therein.

In this section, we explore the potential of such observations for testing GR in a strong-field/high-curvature regime and discriminate GR against EDGB gravity.

First, we concentrate on the case in which two different QPO triplets are measured. We proceed as follows.

1. We fix the BH mass $\bar{M} = 5.3\, M_\odot$ and choose three values for the BH spin ($\bar{a}^\star = 0.05,\, 0.1,\, 0.2$). We then choose values of $\alpha/\bar{M}^2$ consistent with the theoretical bound (15).
2. Using the EDGB equations, we generate two sets of frequencies $\nu_{\rm ref1} = (\nu_\varphi, \nu_{\rm per}, \nu_{\rm nod})_1$ and $\nu_{\rm ref2} = (\nu_\varphi, \nu_{\rm per}, \nu_{\rm nod})_2$ corresponding to two different emission radii $r_1/r_{\rm ISCO} = 1.1$ and $r_2/r_{\rm ISCO} = 1.4$, respectively. As discussed in the Introduction, we assume that these are the QPO frequencies measured by *LOFT*, with corresponding uncertainties, $(\sigma_\varphi, \sigma_{\rm per}, \sigma_{\rm nod})$, 15 times smaller than those measured with the *RXTE*-PCA from GRO J1655-40 (see Equation (2)).
3. We then interpret these simulated data as if they were generated around a Kerr BH, and solve Equations (24)–(26) to infer the values of $(M_j, a_j^\star, r_j)$, $j = 1,2$ corresponding to the two QPO triplets. If the triplets $\nu_{\rm ref1}$, $\nu_{\rm ref2}$ were generated in GR (i.e., with $\alpha/\bar{M}^2 = 0$), then this procedure would yield the same values of the mass and spin parameters ($M_1 = M_2$ and $a_1^\star = a_2^\star$), to within statistical and numerical uncertainties, and truncation error due to neglecting $O(a^{\star 2})$ terms. Conversely, when $\alpha/\bar{M}^2 \neq 0$, it can be expected that different values of $M_1 \neq M_2$ and $a_1^\star \neq a_2^\star$ are derived.

To quantify this discrepancy, we use a Monte Carlo approach. For the selected values of $\bar{M}$, $\bar{a}^\star$, $\alpha/\bar{M}^2$, we consider $2 \times (N = 10^5)$ triplets $(\nu_\varphi, \nu_{\rm per}, \nu_{\rm nod})_{j=1,2}$, with a Gaussian distribution, centered around the values $\nu_{\rm ref1}$ and $\nu_{\rm ref2}$, (computed with the EDGB theory) with standard deviation $(\sigma_\varphi, \sigma_{\rm per}, \sigma_{\rm nod})$.Then, we use Equations (24)–(26) (which assume GR). In Figure 2, we show the distribution of mass (left panel) and spin (right panel) obtained using this procedure, assuming $\bar{M} = 5.3\, M_\odot$, $\bar{a}^\star = 0.10$, and $\alpha/\bar{M}^2 = 0.691$. In order to establish to what extent these distributions are compatible/incompatible with $M_1 = M_2$ and $a_1^\star = a_2^\star$, i.e., with GR, we perform the following analysis.

Let us define

$$\Delta M = M_1 - M_2, \quad \Delta a^\star = a_1^\star - a_2^\star, \quad \Delta r = r_1 - r_2.$$

We verified that the distribution of the variables $\vec{\mu} = (\Delta M, \Delta a^\star, \Delta r)$ is consistent with a Gaussian distribution $\mathcal{N}(\vec{\mu}, \Sigma = \Sigma_1 + \Sigma_2)$ with zero expectation value. We now construct the χ^2 distributed variable with three degrees of freedom:

$$\chi^2 = (\vec{x} - \vec{\mu})^{\rm T}\Sigma^{-1}(\vec{x} - \vec{\mu}); \tag{27}$$

$\chi^2 = c$ defines the ranges of ΔM, $\Delta a^\star$, and Δr at the confidence level specified by c. We use $c = 3.53,\, 8.03,\, 14.16$, which correspond to the 1σ, 2σ, and 3σ confidence levels in a Gaussian distribution equivalent, respectively (i.e., a probability of 32%, 5%, 0.3%).

In the three panels of Figure 3, we show the results of this statistical analysis applied to the case when the two simulated QPO triplets $(\nu_\varphi, \nu_{\rm per}, \nu_{\rm nod})_j$, $j = 1,\, 2$, are computed assuming $\bar{M} = 5.3\, M_\odot$, $\bar{a}^\star = 0.05$, $\bar{r}_j/r_{\rm ISCO} = 1.1,\, 1.4$, and three values of $\alpha/\bar{M}^2$ ($\sim 0,\, 0.576,\, 0.691$).

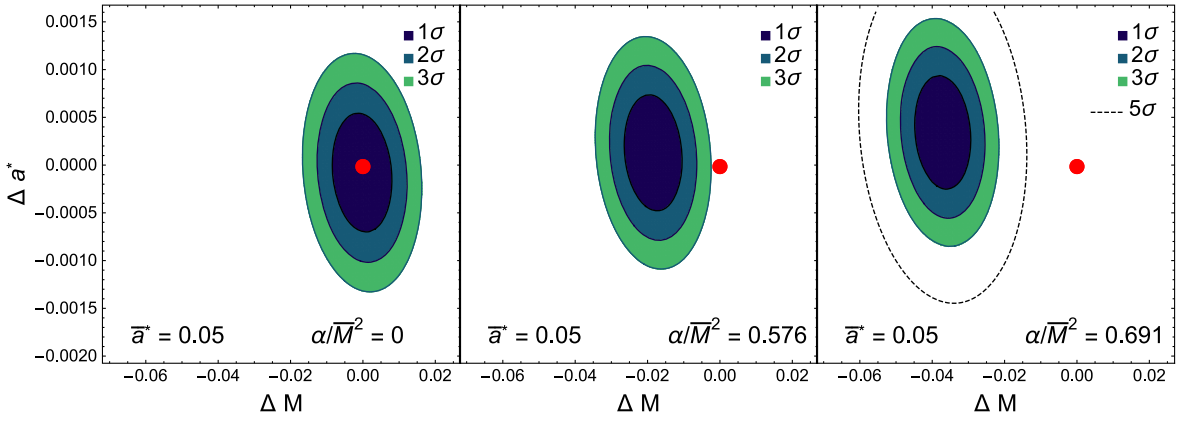

Figure 3. Confidence levels with which GR can be tested against the EDGB theory (see the text) are plotted in the (ΔM, $\Delta a^\star$) plane. The red dot is the origin of the plane. The parameters corresponding to the two injected sets of frequencies $(\nu_\varphi, \nu_{\rm per}, \nu_{\rm nod})_j$ are $\bar{r}_j/r_{\rm ISCO} = 1.1,\ 1.4$, $\bar{M} = 5.3\,M_\odot$, and $\bar{a}^\star = 0.05$. Remember that these frequencies are computed using the EDGB theory. In the left panel, we assume that the coupling constant of the EDGB theory, $\alpha/\bar{M}^2$, is zero, so that the EDGB theory coincides with GR. The red dot falls in the center of the 1σ ellipse, showing that the the two sets of frequencies are fully compatible with GR and that our statistical analysis is correct. In the right panel, we set $\alpha/\bar{M}^2 = 0.691$, i.e., the maximum value allowed by the EDGB theory. The red dot is well outside the 5σ confidence level (dashed line), showing that in this case we would be able to exclude that the two sets of frequencies are generated according to GR. In the middle panel, $\alpha/\bar{M}^2 = 0.576$ and the red dot touches the 3σ confidence level, i.e., the frequencies would be incompatible with GR to this confidence level.

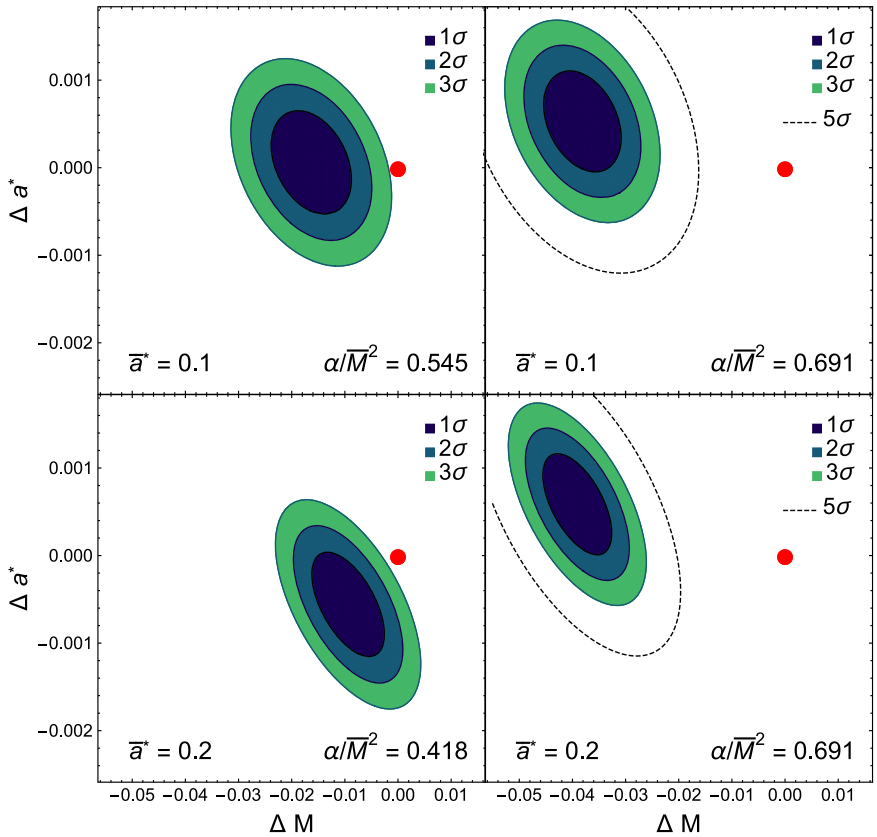

Figure 4. Same as Figure 4, with $\bar{a}^\star = 0.1,\ 0.2$ (upper and lower panels, respectively). $\alpha/\bar{M}^2$ has the maximum value in the right panels, and the threshold value for which GR would be excluded at 3σ confidence level in the left panels.

Each panel shows the regions in the parameter space (ΔM, Δa^*) which correspond to the 1σ, 2σ, and 3σ confidence levels. The red dot corresponds to $\Delta M = 0$, $\Delta a^* = 0$. The left panel refers to the case $\alpha/M^2 = 0$ and the EDGB theory coincides with GR; the ellipses which delimit the confidence levels are centered on the red dots, consistent with two coincident values of M and $a^\star$, i.e., $\Delta M = 0$ and $\Delta a^* = 0$.

Conversely, in the right panel, the largest value of α/M^2 allowed by EDGB theory is used; the red circle lies well outside the 5σ confidence ellipse, demonstrating that the two QPO triplets cannot be interpreted within GR. We note that this simulation is inconsistent with $\Delta M = 0$, but it is still consistent with $\Delta a^\star = 0$. This is due to the fact that the determination of the mass is more sensitive than the determination of the spin to the underlying gravity theory (at least for the slowly rotating BHs with $a^\star \leqslant 0.2$ discussed here).

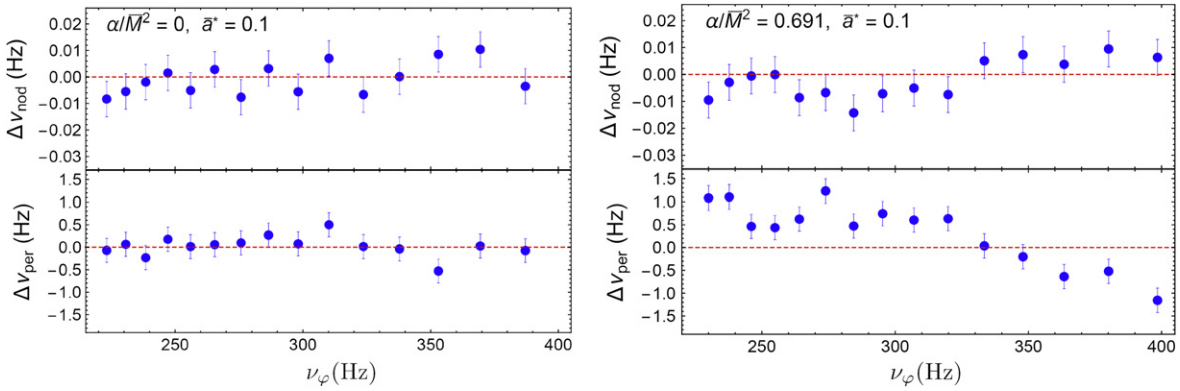

Figure 5. $\Delta_{\rm nod} = (\nu_{\rm nod} - \hat{\nu}_{\rm nod})$ and $\Delta_{\rm per} = (\nu_{\rm per} - \hat{\nu}_{\rm per})$ are shown as functions of the azimuthal frequency ν_φ for BH configurations with $\bar{M} = 5.3 M_\odot$, $\bar{a}^\star = 0.1$, and coupling parameter $\alpha/\bar{M}^2 = (0, 0.691)$. $\hat{\nu}_{\rm per,nod}$ correspond to the periastron and nodal frequencies computed for the best-fit parameters $(\hat{M}, \hat{a}^\star)$, which have been obtained by minimizing the chi-square variable (28). The error bar is 1σ.

Furthermore, Figure 3 shows that for $\alpha/\bar{M}^2 = 0.576$ (middle panel), ΔM would be incompatible with 0 at 3σ. Choosing 3σ as a threshold to assess the compatibility of GR with these simulated data, we conclude that when $\bar{a}^\star = 0.05$, we would be able to discriminate between GR and EDGB theory for values of the coupling constant in the $\alpha/\bar{M}^2 \in (0.576, 0.691)$ range.

In Figure 4, we show plots similar to those in Figure 3 for larger values of the BH angular momentum, i.e., $\bar{a}^\star = 0.1$ (top panels) and $\bar{a}^\star = 0.2$ (bottom panels). We adopt $\alpha/\bar{M}^2 = 0.691$ in the right panels and the values of α/M^2 corresponding to the 3σ threshold, $\alpha/\bar{M}^2 = 0.545$ for $\bar{a}^\star = 0.1$ and $\alpha/\bar{M}^2 = 0.418$ for $\bar{a}^\star = 0.2$ in the left panels. We see that as the BH spin increases, regions of lower α/M^2 can be explored using this method. Therefore, we expect that BHs spinning faster than $a^\star = 0.2$ will allow us to test GR against the EDGB theory for smaller values of the coupling constant.[11]

Let us now discuss the case in which multiple (>2) QPO triplets are detected from the same BH. We adopt the approach of considering two of the QPO frequencies of each triplet as a function of the third frequency (see Figure 5), as is commonly done in observational studies of QPOs (Motta et al. 2014). We adopt the following procedure.

1. We fix $\bar{M} = 5.3 M_\odot$ and $\bar{a}^\star = 0.1$ and choose 15 equally spaced values of r in the range $r = [1.1\text{–}1.6]\, r_{\rm ISCO}$. We then compute two sets of 15 QPO triplets $(\nu_\varphi, \nu_{\rm nod}, \nu_{\rm per})_{j=1,\ldots,15}$ corresponding to $\alpha/\bar{M}^2 = 0$ and $\alpha/\bar{M}^2 = 0.691$.
2. We simulate the QPO frequency triplets by drawing from Gaussian distributions, centered at the frequency values computed in point 1, with the standard deviations expect from observation with the *LOFT*-LAD (see Section 2.1).
3. Using Equation (24), we express the radial coordinate as a function of ν_φ, and the BH mass and spin, $r = r(\nu_\varphi, M, a^\star)$. Replacing this expression into Equations (25)–(26), we obtain the functions $\nu^{\rm GR}_{\rm nod}(\nu_\varphi, M, a^\star)$ and $\nu^{\rm GR}_{\rm per}(\nu_\varphi, M, a^\star)$.
4. For each drawn value of ν_φ (see point 2), we span the $M - a^\star$ parameter space (with $4\, M_\odot \leqslant M \leqslant 10\, M_\odot$ and $0.01 \leqslant a^\star \leqslant 0.2$) and minimize the chi-square variable

$$\chi^2 = \sum_{j=1}^{15} \left[\frac{\left(\nu_{\rm nod} - \nu^{\rm GR}_{\rm nod}\right)^2_j}{\sigma^2_{\rm nod}} + \frac{\left(\nu_{\rm per} - \nu^{\rm GR}_{\rm per}\right)^2_j}{\sigma^2_{\rm per}} \right] \qquad (28)$$

where $\nu_{\rm nod}$ and $\nu_{\rm per}$ are those drawn at point 2. This is equivalent to fitting the dependence of the simulated values $\nu_{\rm nod}$ and $\nu_{\rm per}$ on ν_φ based on GR alone. The χ^2 has average $E[\chi^2] = 2 \times 15 - - 2 = 28$ and standard deviation $\sigma[\chi^2] = \sqrt{2 \times E[\chi^2]} \simeq 7.5$.

The minimum of Equation (28) corresponds to the best-fit parameters $(\hat{M}, \hat{a}^\star)$. For $\alpha/\bar{M}^2 = 0$ we obtain $\chi^2 \simeq 22$, which is within 1σ of the expected value: this indicates that the observed data agree with the theoretical model based on GR predictions. Conversely, for EDGB gravity with maximal coupling $\alpha/\bar{M}^2 = 0.691$, the minimization yields $\chi^2 \simeq 134$, which is incompatible with $E[\chi^2] = 26$ at more than 14σ.

The results of this analysis are shown in Figure 5, where we plot the differences $\Delta\nu_{\rm nod} = (\nu_{\rm nod} - \hat{\nu}_{\rm nod})$ and $\Delta\nu_{\rm per} = (\nu_{\rm per} - \hat{\nu}_{\rm per})$ with $\hat{\nu}_{\rm per/nod} = \nu^{\rm GR}_{\rm per}\big/{\rm nod}(\nu_\varphi, \hat{M}, \hat{a}^\star)$. The left panel shows that for $\alpha/\bar{M}^2 = 0$, both $\Delta\nu_{\rm nod}$ and $\Delta\nu_{\rm per}$ fluctuate around zero to within $\sim 1\sigma$. For $\alpha/\bar{M}^2 = 0.691$ (right panel) a clear trend is apparent, especially in $\Delta\nu_{\rm per}$, as a function of the azimuthal frequency ν_φ.

5. CONCLUDING REMARKS

In this article, we have shown that the QPO frequencies can be used to test GR against alternative theories of gravity, in the strong-field/high-curvature regime, and to derive constraints on the parameters that characterize these theories. In particular, we have considered one of the best motivated alternatives to GR, i.e., the EDGB theory, and we have adopted for the QPOs the Relativistic Precession Model. We have shown that the high sensitivity of the proposed ESA M-class mission *LOFT* can provide stringent constraints on the parameter α/M^2 which characterizes this theory. These constraints would be stronger than current observational bounds coming from the orbital

[11] It should be noted that our results for $a^\star = 0.2$ are to be considered as an extrapolation since, as mentioned above, we neglected terms of the order of $O(a^\star)^2$; in a subsequent paper, we will generalize the EDGB BH solution and extend our analysis to consistently include second-order terms in the BH spin.

decay rate of low-mass X-ray binaries (Yagi (2012), see Section 3.2) by a factor of $\sim 4-5$.

Our analysis was carried out considering slowly rotating BHs ($a^\star \lesssim 0.2$). Since more stringent constraints on α/M^2 can be found for larger values of the black hole spin, we plan to extend this work to include higher-order spin corrections. Moreover, in a future study, we will consider alternative QPO models.

L.S. acknowledges partial support from PRIN-INAF 2011. P.P. acknowledges support from FCT-Portugal through project IF/00293/2013.

REFERENCES

Abramowicz, M. A., & Kluźniak, W. 2001, A&A, 374, L19
Abramowicz, M. A., & Kluzniak, W. 2003, GReGr, 35, 69
Alexander, S., & Yunes, N. 2009, PhR, 480, 1
Amaro-Seoane, P., Gair, J. R., Pound, A., Hughes, S. A., & Sopuerta, C. F. 2014 (arXiv 1410.0958)
Ayzenberg, D., & Yunes, N. 2014, PhRvD, D90, 044066
Bambi, C. 2012, JCAP, 1209, 014
Bambi, C. 2013a, JCAP, 1308, 055
Bambi, C. 2013b, arXiv:1312.2228
Bambi, C., & Barausse, E. 2011, ApJ, 731, 121
Beer, M. E., & Podsiadlowski, P. 2002, MNRAS, 331, 351
Belloni, T. M., & Stella, L. 2014, SSRv, 183, 43
Casella, P., Belloni, T., & Stella, L. 2005, ApJ, 629, 403
Chandrasekhar, S. 1984, in The Mathematical Theory of Black Holes, Oxford Classic Texts in the Physical Sciences (Oxford: Oxford Univ. Press)
Collins, N. A., & Hughes, S. A. 2004, PhRvD, 69, 124022
Damour, T., & Esposito-Farèse, G. 1993, PhRvL, 70, 2220
Fabian, A. C. 2013, in IAU Symp., 290, Feeding Compact Objects: Accretion on All Scales, ed. C. M. Zhang, T. Belloni, M. Méndez, & S. N. Zhang (Paris: IAU), 3
Feroci, M., Stella, L., van der Klis, M., et al. 2012, ExA, 34, 415
Fujii, Y., Maeda, K., et al. 2003, in The scalar-tensor theory of gravitation (Cambridge: Cambridge Univ. Press)
Gierliński, M., Middleton, M., Ward, M., & Done, C. 2008, Natur, 455, 369
Glampedakis, K., & Babak, S. 2006, CQGra, 23, 4167
Hawking, S. W., & Ellis, G. F. R. 1973, in The Large Scale Structure of Space-Time, Cambridge Monographs on Mathematical Physics (Cambridge: Cambridge Univ. Press)
Johannsen, T., & Psaltis, D. 2010, ApJ, 716, 187
Johannsen, T., & Psaltis, D. 2011, ApJ, 726, 11
Johannsen, T., & Psaltis, D. 2013, ApJ, 773, 57
Kanti, P., Mavromatos, N., Rizos, J., Tamvakis, K., & Winstanley, E. 1996, PhRvD, 54, 5049
Kluzniak, W., & Abramowicz, M. A. 2001, AcPPB, 32, 3605
Kramer, M. 2014, IJMPD, 23, 30004
McClintock, J. E., Narayan, R., Davis, S. W., et al. 2011, CQGrav, 28, 114009
Merloni, A., Vietri, M., Stella, L., & Bini, D. 1999, MNRAS, 304, 155
Mignemi, S., & Stewart, N. 1993, PhRvD, 47, 5259
Motta, S., Belloni, T., Stella, L., Muñoz-Darias, T., & Fender, R. 2014, MNRAS, 437, 2554
Moura, F., & Schiappa, R. 2007, CQGra, 24, 361
Özel, F., Psaltis, D., Narayan, R., & McClintock, J. E. 2010, ApJ, 725, 1918
Pani, P., Berti, E., Cardoso, V., & Read, J. 2011a, PhRvD, 84, 104035
Pani, P., & Cardoso, V. 2009, PhRvD, 79, 084031
Pani, P., Macedo, C. F., Crispino, L. C., & Cardoso, V. 2011b, PhRvD, 84, 087501
Psaltis, D. 2008, LRR, arXiv:0806.1531
Psaltis, D. 2009, JPhCS, 189, 012033
Sotiriou, T. P., & Faraoni, V. 2012, PhRvL, 108, 081103
Sotiriou, T. P., & Zhou, S.-Y. 2014, PhRvL, 112, 251102
Stella, L., & Vietri, M. 1998, ApJL, 492, L59
Stella, L., & Vietri, M. 1999, PhRvL, 82, 17
Stella, L., Vietri, M., & Morsink, S. M. 1999, ApJL, 524, L63
Syunyaev, R. A. 1972, AZh, 49, 1153
van der Klis, M. 2000, ARA&A, 38, 717
van der Klis, M. 2006, in Rapid X-ray Variability, ed. W. Lewis & M. van der Klis (Cambridge: Cambridge Univ. Press), 39
Vigeland, S., Yunes, N., & Stein, L. 2011, PhRvD, 83, 104027
Vincent, F. 2013, CQGra, 31, 025010
Wald, R. M. 2010, in General relativity (Chicage, IL: Univ. Chicago press)
Will, C. M. 2014, LRR, 17, 4
Woodard, R. P. 2007, LNP, 720, 403
Yagi, K. 2012, PhRvD, 86, 081504
Yunes, N., & Siemens, X. 2013, LRR, 16, 9
Yunes, N., & Stein, L. C. 2011, PhRvD, 83, 104002